Microchemical Journal 142 (2018) 159–166

Contents lists available at ScienceDirect

Microchemical Journal

journal homepage: www.elsevier.com/locate/microc

Nickel nanowires-based composite material applied to the highly enhanced non-enzymatic electro-oxidation of ethanol

Cecilia S. Tettamanti[a], María L. Ramírez[a], Fabiana A. Gutierrez[a], Paula G. Bercoff[b], Gustavo A. Rivas[a], Marcela C. Rodríguez[a,*]

[a] Departamento de Fisicoquímica, Facultad de Ciencias Químicas, Universidad Nacional de Córdoba, INFIQC, CONICET, Córdoba, Argentina
[b] Facultad de Matemática, Astronomía, Física y Computación, Universidad Nacional de Córdoba. IFEG, CONICET. Córdoba, Argentina

ABSTRACT

In this work, we report the building of a nanostructured platform with activity towards the non-enzymatic oxidation of ethanol. This nanostructured platform was obtained by including Ni nanowires (NiNWs) in a graphite matrix composite. The NiNWs were obtained by electrochemical synthesis using commercial aluminum oxide templates and characterized by scanning electronic microscopy (SEM), X-ray emission (EDS) and X-ray diffraction (XRD). The composite transducer (CPE-NiNWs) was studied by cyclic voltammetry, amperometry and electrochemical impedance spectroscopy (EIS) assays. CPE-NiNWs proved to be highly sensitive for the detection of ethanol in 0.10 M NaOH, demonstrating a wide linear range (1.0×10^{-4}–1.1×10^{-2} M) and a detection limit of 3.10×10^{-7} M. CPE-NiNWs was used for the efficient quantification of ethanol in distilled alcoholic beverages, obtaining results comparable to those reported by the manufacturers. The operational conditions of CPE-NiNWs were accomplished in terms of the best analytical performance for non-enzymatic quantification of ethanol. CPE-NiNWs demonstrated a very good short-term stability (for 5 successive determinations using the same surface), proving an outstanding long-term stability, allowing its use for at least 60 days.

1. Introduction

In our days, the primary need of powerful portable analytical tools with high sensitivity and reliability, fast response, selectivity, accuracy, lower fabrication and reagent costs, reduced waste production and samples consumption is a subject of central interest to be addressed [1–5].Particularly, chemical sensors and biosensors have emerged as versatile tools in the field of environmental control, hazardous materials detection, pharmaceutics, industry, food safety and clinical diagnostics [6–10].In this way, the biggest challenge in biosensors development is the successful construction of a biospecific surface, sensitive and selective for a particular analyte, able to produce detectable signals that may be collected by a suitable transductor (i.e. electrochemical, optical, piezoelectric) [3, 11–13]. However, the handling of biomolecules during the construction of the biospecific surface is a hard issue to be solved [14, 15]. The immobilization process of the functional biomolecule in many cases affects its recognition properties influencing the biosensor sensitivity and, sometimes, also selectivity may be compromised, mainly in harsh working environment, such as extreme pH values. In these limit cases, some nanomaterials can be used in replacement of weak and costly biomolecules. A large number of different nanomaterials offer outstanding properties, such as fast electron transfer kinetics, high surface-to-volume ratio, chemical stability even in harsh environments and the possibility of mimicking biomolecular events [16–18]. Therefore, nanomaterials have been employed in the design of functional surfaces in order to boost the recognition event and signal transduction due to their outstanding inherent electron transfer properties [19–22].These functional nanomaterials have attracted great attention in the last years due to their several advantages like good stability and effective catalysis [23, 24]. Nanomaterials containing nickel species in their composition are the most commonly used non-noble metal catalysts with a wide range of sizes and shapes. Diverse nickel nanomaterials have been employed in numerous electrochemical sensing systems [25–27], design of fuel cells [28, 29], alkaline batteries [30, 31] and supercapacitors [32, 33], demonstrating their high intrinsic efficiency as oxidation reaction enhancers for alcohols in alkaline conditions [34].

The complex surface chemistry of Ni in alkaline solutions and its oxidation states strongly influence its catalytic activity, performance and therefore, efficiency [35–37]. Furthermore, there are strong evidences that Ni hydroxides are distinctly electron mediators in electrochemical applications due to their remarkable catalytic activity owing

* Corresponding author.
E-mail address: marcela.rodriguez@fcq.unc.edu.ar (M.C. Rodríguez).

https://doi.org/10.1016/j.microc.2018.06.023
Received 16 March 2018; Received in revised form 12 June 2018; Accepted 12 June 2018
Available online 21 June 2018
0026-265X/

to the formation of the Ni(II)/Ni(III) redox couple on the surface of the electrode, as compared to other metal oxide nanomaterials [35–37]. Likewise, the anti-poison power of nickel and its long-term stability in alkaline solutions make it an attractive candidate for many Ni-based electrocatalytic applications [38, 39].

In this work, we propose the use of nickel nanowires (NiNWs) as catalytic nanomaterial, taking advantage of their high oxidation activity towards ethanol. NiNWs were prepared by electrochemical synthesis using alumina membranes (AAO) and included in a carbon paste electrode material (CPE-NiNWs). In the following sections, we explore the catalytic activity of untreated and electrochemically pretreated CPE-NiNWs towards sensitive ethanol sensing in alkaline conditions and its applicability as a nanostructured system.

2. Experimental

2.1. Reagents and materials

Ethyl alcohol absolute anhydrous (99.88%) and sodium hydroxide (pellets) were provided from J.T. Baker. Nickel(II) chloride hexahydrate, nickel(II) sulfamate tetrahydrate (98%) and mineral oil were purchased from Sigma-Aldrich, while graphite powder (grade #38) was acquired from Fischer Scientific. Copper (I) chloride was provided from Dalton. Anodisc alumina membranes (AAO), with a mean pore diameter of 200 nm and thickness of 60 μm, were obtained from Whatman®.Ultrapure water ($\rho = 18.2\ M\Omega\ cm$) from Millipore-MilliQ system was used for the preparation of all solutions in this work. A solution of0.10 M NaOH was used as supporting electrolyte. All measurements were performed at room temperature.

2.2. Apparatus

Electrochemical measurements were performed with TEQ 04 and Autolab PGSTAT 30 potentiostats. EIS were performed in the frequency range between 10 KHz and 10 MHz, with a potential perturbation of 10 mV and a working potential of 0,550 V using an ethanol solution. The impedance spectra were analyzed by using the z-view software. Reference Ag/AgCl/NaCl and a platinum wire counter electrodes were provided by CH Instruments. The working electrode was a Teflon® body with a stainless-steel screw to establish the electric contact with the carbon paste. The electrodes were inserted into the cell through holes in its Teflon cover. A magnetic stirrer provided the convective transport during the amperometric measurements.

Nickel nanowires (NiNWs) were characterized by scanning electron microscopy (SEM) and X-ray diffraction. A Sigma Zeiss Field Emission scanning electron microscope with an Oxford energy dispersive (EDS) detector (LAMARX facilities) was used to characterize the morphology -through secondary and backscattered electrons images- and the elemental composition of the samples. X-ray diffraction (XRD) patterns were measured with a PANalytical X'Pert PRO powder diffractometer (operating at 40 kV, 40 mA), in Bragg–Brentano reflection geometry with CuKα radiation ($\lambda = 1.5418$ Å). The data were obtained in the 2θ range between 8° and 120° in steps of 0.02°, using PIXcel detector.

2.3. Nickel nanowires synthesis

AAO membranes were used as templates for the electrodeposition of NiNWs($\sim 9 \times 10^9$/membrane) [40]. Previous to the synthesis procedure, the membranes were sputtered with a ~85 nm copper film on one side to provide electrical contact. NiNWs were prepared by electrochemical deposition, into the pores of the membranes, using an aqueous solution of 515 g/L $Ni(H_2NSO_3)_2{\cdot}4H_2O$; 20 g/L $NiCl_2{\cdot}6H_2O$and 20 g/L H_3BO_3, applying −1.20 V vs. Ag/AgCl electrode, until reaching an electrodeposition charge of 20C [41]. After electroplating, the copper layer was dissolved in a 0.5 M CuCl solution (30% HCl). Finally, the AAO template was immersed in 3 M NaOH for 30 min in order to release the NiNWs. Later, the NiNWs were washed with ultrapure water and then stored as an aqueous dispersion.

2.4. Preparation of the working electrodes

The carbon paste electrode (CPE) was prepared by mechanical mixing of graphite powder (70.0% w/w) and mineral oil (30.0% w/w) in an agate mortar for 30 min. CPEs containing NiNWs were prepared as follows: an appropriate volume of NiNWs dispersion ($\sim 18.0 \times 10^9$ NiNWs/mL) was added to the graphite and heated at 100 °C for 1 h to complete the water evaporation. This step was followed by the incorporation of the mineral oil and mixing for additional 30 min. A portion of the resulting paste was firmly packed into the cavity of a Teflon tube (3 mm diameter). The electrical contact was established through a stainless steel screw. A new surface was obtained by smoothing the electrode onto a weighing paper before starting each new experiment.

Three composites were prepared containing different amounts of NiNWs: CPE 4.5M-NiNWs ($\sim 4.5 \times 10^6$ NiNWs/mg CPE), CPE 9.0M-NiNWs ($\sim 9.0 \times 10^6$ NiNWs/mg CPE) and CPE 18.0M-NiNWs ($\sim 18.0 \times 10^6$ NiNWs/mg CPE).

Previous to each electrochemical measurement, CPE-NiNWs electrodes were pretreated by performing 10 potential cycles between −0.200 V and 0.800 V at 0.100 Vs^{-1} in 0.10 M NaOH.

3. Results and discussion

3.1. Structural characterization: morphological studies by SEM and XRD

Fig. 1 depicts SEM backscattered electrons (BSE) images obtained from the nanocomposites with different amounts of NiNWs: (CPE 4.5M-NiNWs) (a), (CPE 9.0M-NiNWs) (b) and (CPE 18.0M-NiNWs) (c). NiNWs appear brighter than the carbon matrix due to Z-contrast. It is clear from the pictures that NiNWs are uniformly distributed within the matrix, even when the number of NiNWs increases in the composite. Fig. 1.SI (Supporting information) reveals the homogeneous size distribution of NiNWs that exhibit a mean length of ~30 μm and a mean diameter of ~200 nm.

Several EDS spectra were measured from different areas of the samples in order to improve statistical uncertainties related to the speciation and quantification of the elements present in the composite. A representative secondary electrons (SE) image and the corresponding EDS spectrum of CPE-NiNW scan be observed in Fig. 1.d and .e, respectively. Beside the carbon corresponding to the composite, only nickel and oxygen are detected in a Ni:O atomic ratio of 100:22. This result indicates that no impurities remained after the synthesis and hints the presence of a small amount of nickel oxide and/or hydroxide, probably produced during the releasing process of the NiNWs from the AAO template. In order to verify this hypothesis, XRD was performed on the as-released NiNWs (before preparing the composites). Fig. 2.SI shows the corresponding XRD pattern, where the main peaks of the fcc structure of metallic Ni have been indexed, in accordance to JCPDS file No. 04-0850. A highly crystalline structure is obtained with no traces of nickel oxide and a very small amount of $Ni(OH)_2$, which is noticed in the inset. The appearance of this phase is in accordance with the oxygen detected by EDS experiments.

3.2. Electrochemical characterization of NiNWs-CPE

As it is widely known [42, 43],nickel spontaneously forms $Ni(OH)_2$, following the reaction described in Eq. (1).

$$Ni_{(s)} + 2H_2O_{(l)} \rightleftharpoons Ni(OH)_{2(s)} + 2H_{2(g)} + 4e^- \quad (1)$$

In order to evaluate the electrochemical behavior of the NiNWs included in the CPE (NiNWs-CPE), cyclic voltammetry experiments were done performing 10 consecutive cycles keeping constant the

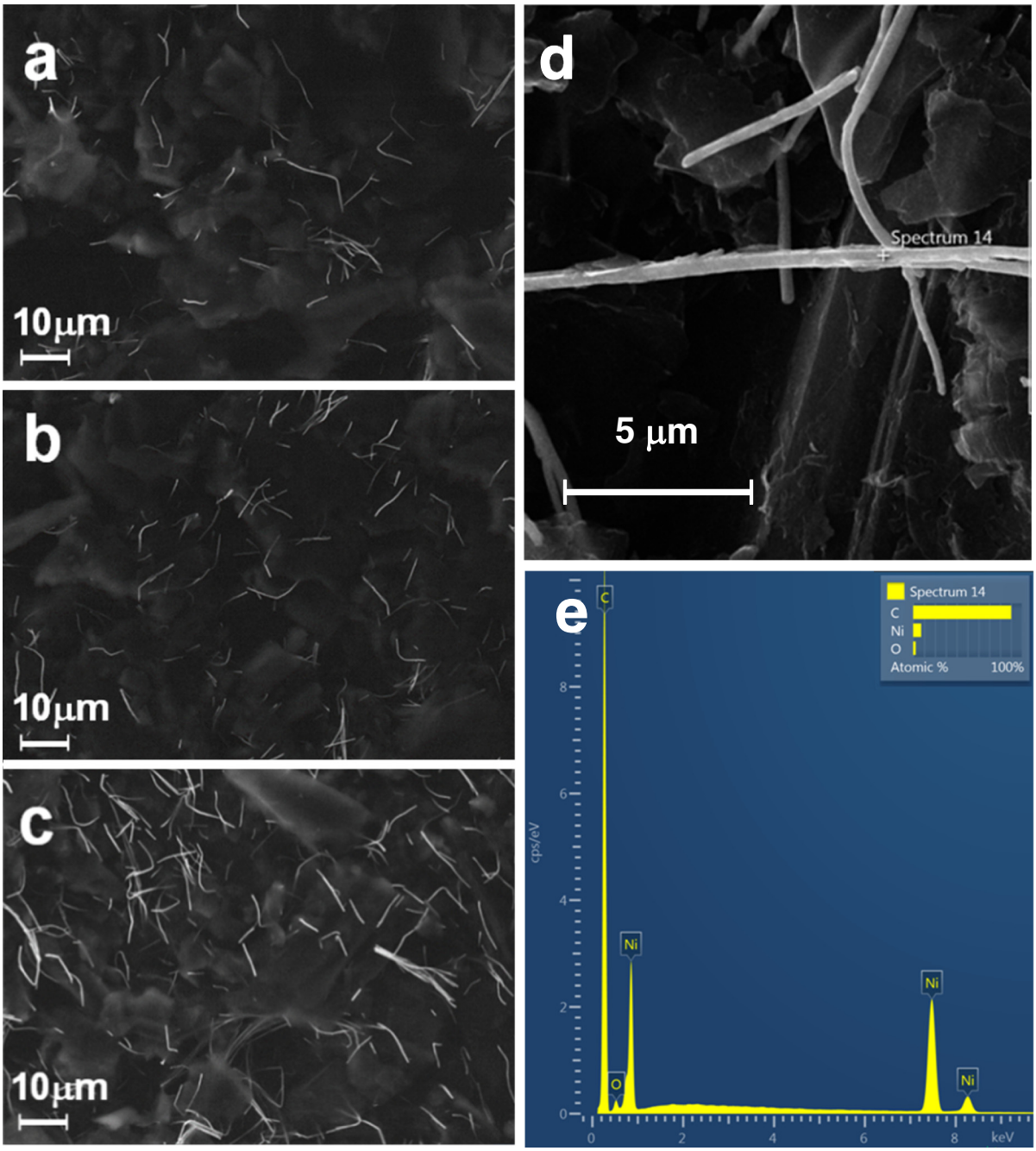

Fig. 1. SEM backscattered electrons (BSE) images obtained from the nanocomposites. CPE 4.5M-NiNWs (a), CPE 9.0M-NiNWs (b) and CPE 18.0M-NiNWs (c). Secondary electrons (SE) image of CPE 18.0M-NiNWs at higher magnification (d) EDS spectrum performed on a single NiNW (e).

cathodic limit (−0.200 V) and changing the anodic limit to 0.400, 0.500, 0.600, 0.700 and 0.800 V. For easy understanding, Fig. 3.SI shows only the last cycle (cycle #10) of each experiment. As it can be seen, when the anodic limit is 0.400 V (a) there is no definition of the redox behavior of Ni species. A similar profile is found for 0.500 V (b), while for 0.600 V (c), the redox process takes place (inset of Fig. 3.SI). When the anodic limit reaches more positive potentials, the redox process becomes more evident (d and e). The maximum peak current for both process is achieved at the limit of 0.800 V. At potentials higher than 0.800 V, the oxidation of the supporting electrolyte becomes more important, therefore, the anodic limit for further experiments was fixed at 0.800 V.

In the interest of evaluating a possible pretreatment to obtain the best sensitivity, related to the amount of catalyst electrogenerated at the electrode surface, cyclic voltammetry experiments were done performing consecutive cycles, analyzing the rising of the current peak vs. cycles number. Fig. 2 shows the voltammetry response of ten consecutive cycles for NiNWs-CPE. It is possible to observe current peaks corresponding to the redox processes of Ni species. In the first cycle (a), there is a very small (almost indistinguishable) anodic current associated to the oxidation process of $Ni(OH)_2$ (spontaneously generated Eq. (1)) to NiOOH (Eq. (3)). At higher potentials than the process previously described, oxidation of Ni (0) to $Ni(OH)_2$ occurs (Eq. (2)). In the reverse scan, a cathodic process can be observed, corresponding to the reduction of NiOOH [44]. From the second (b) to the tenth (j) scan, it is possible to notice that the anodic process becomes more evident and defined; the same feature can be seen for the cathodic process. Successive cycles contribute to the enrichment of Ni hydroxides in the

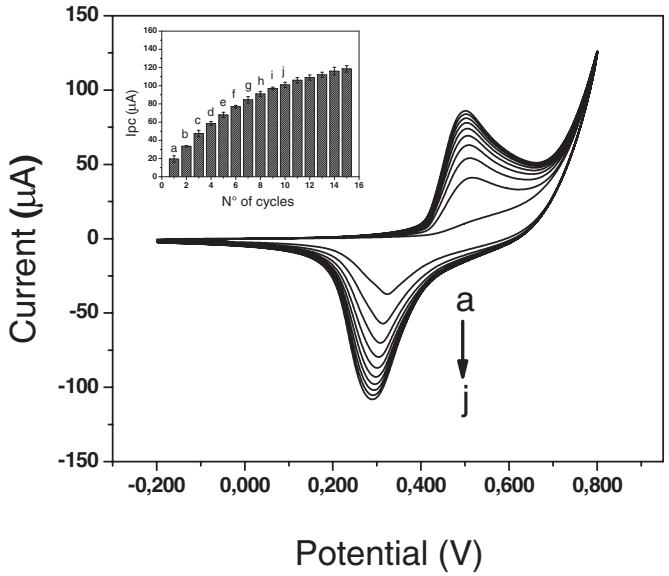

Fig. 2. Consecutive cyclic voltammograms for CPE 18.0M-NiNWs. Supporting electrolyte: 0.100 M NaOH. Scan rate: 0.100 V s^{-1}. Inset: plot of cathodic peak current values vs number of cycles.

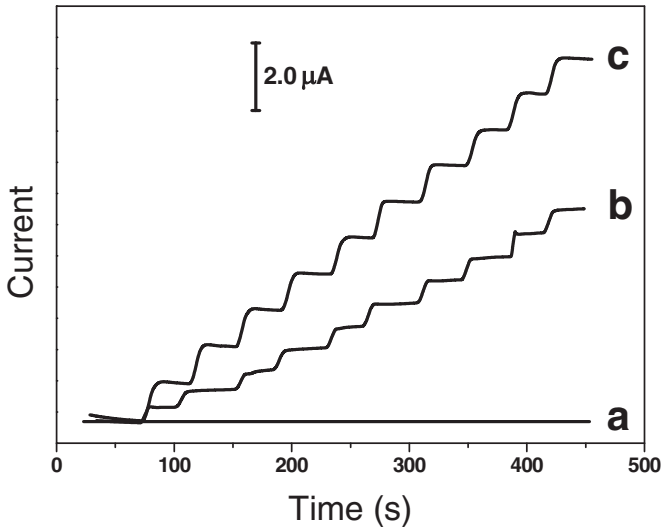

Fig. 3. Amperometric recordings for ethanol electro-oxidation at different electrode surfaces: bare CPE (a), un-treated CPE 18.0M-NiNWs (b), and electrochemical pre-treated CPE 18.0M-NiNWs (c). Supporting electrolyte: 0.100 M NaOH. Working electrode potential: 0.550 V. Ethanol additions: 1.0×10^{-3} M.

electrode surface [36].

$$Ni_{(s)} + 2OH^-_{(ac)} \rightleftharpoons Ni(OH)_{2(s)} + 2e^- \quad (2)$$

$$Ni(OH)_{2(s)} + OH^-_{(ac)} \rightleftharpoons NiOOH_{(s)} + H_2O_{(l)} + e^- \quad (3)$$

As it can be seen in the inset of Fig. 2, cathodic current peaks increase considerably from the first (a) to the tenth (j) cycle reaching an almost constant value for the successive cycles. Therefore, to ensure the largest possible amount of the nanocatalyst at the surface, in the following experiments the electrode surface was previously pre-treated performing 10 cycles, from −0.200 V to 0.800 V, in NaOH 0.10 M.

In order to evaluate the importance of the pretreatment, a complementary assay was performed by amperometric experiments for ethanol electro-oxidation. As mentioned previously, NiOOH is generated at the electrode surface by the electrochemical pretreatment, being this species the responsible for electro-catalyzing the oxidation of ethanol (Eq. (4)).

$$4\,NiOOH + CH_3CH_2OH + OH^-_{(ac)} \rightleftharpoons CH_3COO^- + 4\,Ni(OH)_2 \quad (4)$$

The experiments were done at 0.550 V, comparing the amperometric response of CPE (bare), untreated and electrochemical pretreated CPE 18.0M-NiNWs (Fig. 3). As it can be seen, for CPE (a) a flat response is obtained upon 10 successive additions of 1.0×10^{-3} M ethanol. This profile is consistent with the absence of the catalyst, since the electrode surface is not reactive towards ethanol. For untreated CPE 18.0M-NiNWs (b) there is a defined response upon the addition of ethanol. However, if the CPE 18.0M-NiNWs is pretreated (c), the response for ethanol is higher and better defined, proving that the pretreatment is needed to allow the formation of a bigger amount of Ni $(OH)_2$ and NiOOH species on the NiNWs present in the composite, resulting in an increase of the electrocatalytic layer.

In order to find the optimal conditions for the electrocatalytic oxidation of ethanol, hydrodynamic voltammograms for 3.0×10^{-3} M ethanol in 0.100 M NaOH were performed for different composites. Fig. 4 displays the behavior of CPE (a) and CPE 18.0M-NiNWs (b). As expected, no response is obtained for CPE. Therefore, (as it was concluded before) the presence of the nanocatalyst is needed for the ethanol oxidation process. For CPE 18.0M-NiNWs there is no response from 0.100 V to 0.400 V indicating that, even in the presence of the nanocatalyst, the surface is not reactive in this potential range. The ethanol electro-oxidation starts at 0,450 V over CPE 18.0M-NiNWs,

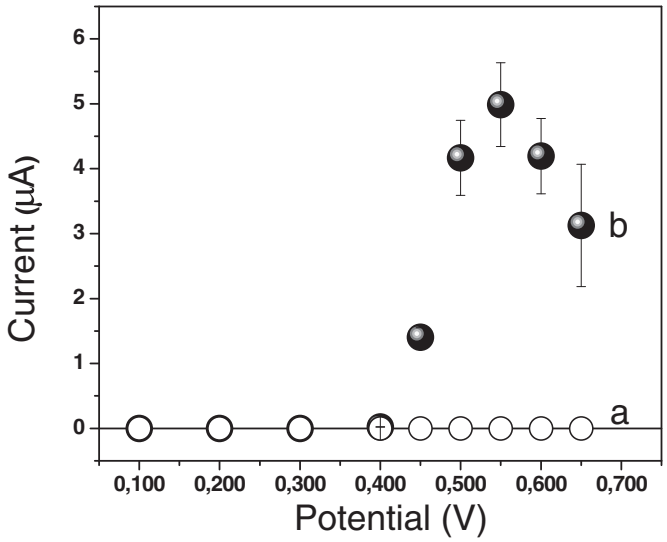

Fig. 4. Hydrodynamic voltammograms obtained for bare CPE (a) and CPE 18.0M-NiNWs (b) electrodes for 3.0×10^{-3} mol L^{-1} ethanol. Supporting electrolyte: 0,100 M NaOH.

reaching its maximum value at 0.550 V, being this value the selected potential for further experiments.

The following experiments were focused on the critical study of the amount of NiNWs contained in the composite. For this purpose, three different composites using different amounts of NiNWs were evaluated by EIS using the previously optimized conditions. Fig. 5 displays the Nyquist plots obtained at 0.550 V for CPE (a, upper inset), CPE 4.5M-NiNWs (b), CPE 9.0M-NiNWs (c) and CPE 18.0M-NiNWs (d) in the presence of 0.050 M ethanol in 0.10 M NaOH. The experimental data (symbols) demonstrate a very good agreement with the fitting data obtained by the equivalent circuit ($R_s(R_{ct}C_{dl})$) (solid lines), where R_{ct} is the charge transfer resistance, C_{dl} is the double layer capacitance, and R_s is the electrolyte resistance. As it can be seen, R_{ct} decreases when CPE is modified with NiNWs, being the R_{ct}: $(7 \pm 2) \times 10^6$, $(15.8 \pm 0.3) \times 10^3$, $(11 \pm 2) \times 10^3$ and $(3.6 \pm 0.2) \times 10^3\,\Omega$, for CPE, CPE 4.5M-NiNWs, CPE 9.0M-NiNWs and CPE 18.0M-NiNWs, respectively. The large decrease in R_{ct} obtained for CPE 18M-NiNWs

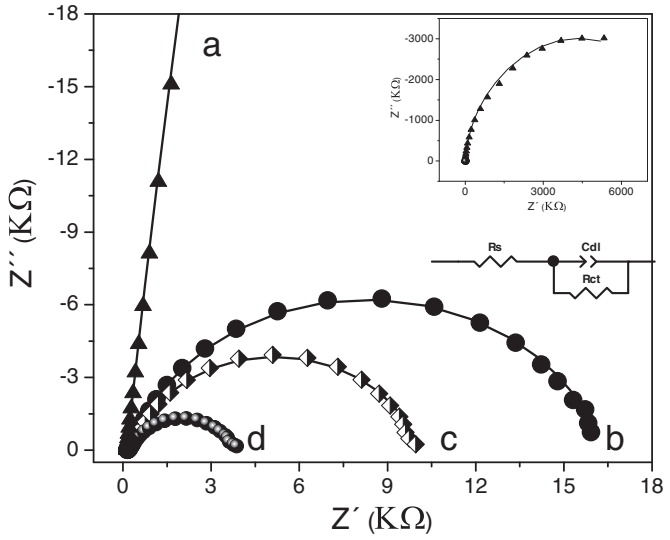

Fig. 5. Nyquist plots for the impedance spectra for CPE (a, upper inset) and CPE modified with 4.5M-NiNWs (b), CPE 9.0M-NiNW (c) and CPE 18.0M-NiNW (d). Frequency range: 1.0×10^{-1}–1.0×10^{5} Hz, potential perturbation: 0.010 V, working electrode potential: 0.550 V. Ethanol solution: 0.050 M. Supporting electrolyte: 0.10 molL^{-1} NaOH. Lower inset: equivalent circuit used for fitting the EIS data.

confirms the catalytic activity towards ethanol electro-oxidation, as it was previously demonstrated by amperometry. The important enhancement of sensitivity and the drastic decrease of R_{ct} for ethanol electro-oxidation clearly demonstrate the key role of the amount of NiNWs present in the composite electrode on the electrocatalytic activity. For further experiments, the selected amount of NiNWs was 18.0M-NiNWs, considering the best compromise between signal-to-noise ratio, sensitivity, R_{ct}, stability of the signal and response time.

3.3. Analytical performance of CPE 18.0M-NiNWs

In order to evaluate the performance of the non-enzymatic electro-oxidation of ethanol at CPE 18.0M-NiNWs, amperometric experiments were carried out. Fig. 6 depicts the amperometric recordings for 10 successive additions of 1.0×10^{-4} M followed by 10 successive additions of 1.0×10^{-3} M of ethanol. As it is evident from Fig. 6, a fast and well-defined response is observed after each addition of ethanol. The response reaches 90% of the steady-state current in 11 s. The corresponding calibration plot is depicted in the inset. The linear range goes from 1.0×10^{-4} M to at least up to 1.1×10^{-2} M. The analytical parameters are the following: sensitivity (1372 ± 4) μAM^{-1} (R^2 = 0.9999), detection limit: (3.1×10^{-7}) M (LOD assumed as (3σ)/S, where σ is the standard deviation of the blank signal and S the sensitivity), while the quantification limit (LOQ, taken as 10 σ/S), is 9.4×10^{-7} M.

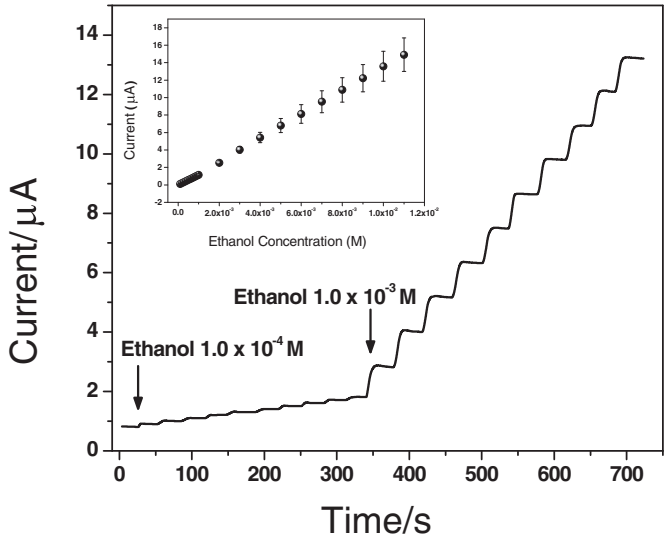

Fig. 6. Amperometric recording at CPE 18.0M-NiNWs electrode for 10 additions of ethanol 1.0×10^{-4} M followed by 10 additions of ethanol 1.0×10^{-3} M. Supporting electrolyte: 0.100 M NaOH. Working electrode potential: 0.550 V. Inset: corresponding calibration plot.

Information about the analytical parameters of different ethanol electrochemical sensors and biosensors reported in the recent years is summarized in Table 1. This platform presents a LOD and LOQ lower than most of the reported sensors [27, 38, 45, 46]. Even when a strict comparison of sensitivities is not possible, the results obtained with our platform are similar or better than those presented in Table 1. The linear range obtained under the working conditions is comparable to the rest of the sensors systems in terms of orders of magnitude [27, 47, 48].It is worth to mention that, in addition to its excellent performance, the proposed platform exhibits outstanding operational properties when compared to the rest of the reported electrochemical devices. One of the main advantages of this platform is its high robustness, unlike enzymatic sensing systems [45, 46] shown by the long-term stability (60 days) at room temperature [27, 38, 45–48].

Operational stability of the sensor under continuous use was evaluated through five successive amperometric experiments for 10 additions of 1.0×10^{-3} M ethanol, performed using the same electrode surface. Fig. 4.SI shows the ratio between the sensitivity values of successive calibration curves normalized to the first calibration. As it can be seen in this figure, all the values are close to 1(1.06 ± 0.05). It is worth mentioning that each calibration measurement takes around 10 min, and after 5 assays with the same surface, the working time of the electrode reaches almost 1 h keeping the sensitivity close to the initial value, with an excellent reproducibility.

The long-term stability of the prepared and stored at room temperature electrode material was evaluated. The nanocomposite CPE 18.0M-NiNWs was prepared and used along 60 days (Fig. 5.SI), testing its sensitivity on the first day and comparing with the sensitivities values of days10, 20, 30 and 60 (every day the experiments were performed by triplicate). Fig. 5.SI depicts the normalized sensitivities with respect to that of the first day, with an average value of (1.02 ± 0.07), demonstrating an outstanding reproducibility along a period of at least 60 days. This result proves the robustness of the nanomaterial inside the composite and its ability to maintain the catalytic behavior as the first day, unlike enzymes or other biomolecules.

In order to consider further analytical applications of CPE 18.0M-NiNWs for non-enzymatic ethanol electro-oxidation, as a proof of concept, the platform was challenged with two complex alcoholic beverage samples using this composite electrode. The assayed beverages were Cane brandy (51®) and Vodka (Absolut®), provided by a local market. The concentration obtained with our sensor was (39 ± 1) % v/v and (40 ± 1) % v/v for Cane brandy and Vodka beverages, respectively, demonstrating very good agreement with the value reported in the product label (39% v/v for Cane brandy and 40% v/v for Vodka, respectively).

The selectivity of the sensor towards glucose and sulphite anion was also evaluated, tacking the same experimental conditions assayed for the real samples. Even when glucose is not present in distilled beverages [49], we have evaluated the interference of an addition corresponding to 5.5 g/L glucose compared to the signal obtained for an addition corresponding to 39.0% v/v ethanol solution (as in the most common distilled beverages). The interference of glucose was just 6.7% of the response of ethanol (Fig. 6 SI A). We have also evaluated the interference of sulphite anion, which is a common additive used as preservative or antioxidant in food and beverages [50–52].The sensor

Table 1
Analytical performance comparison of CPE 18.0M-NiNWs with different reported platforms for ethanol detection.

Sensor/biosensor	Method	Sensitivity	LOD-LOQ	Dynamic linear range	R^2	Comments	Ref.
CPE/NiO-NDs	Amperometry +0.6 V Electrolyte: 0.15 M NaOH containing 0.1 M KCl	3.51 μA mM^{-1} cm^{-2} [(3.51 × 10^3 μA M^{-1} cm^{-2})][a]	1 mM-N/A [1 × 10^3 μM-N/A][a]	1–47 mM [(1–47) × 10^{-3} M][a]	0.99735	Real samples: N/A Operational stability: N/A Long-term stability: N/A	[27]
SPCE/RA/ADH + NAD^+	Amperometry +0.20 V Electrolyte: PBS pH 7.75	1.36 μA mM^{-1} [(1.36 × 10^3 μA M^{-1})][a]	7.1 μM-23.7 μM	23.71–1000 μM [(23.71–1000) × 10^{-6} M][a]	0.9994	Real samples: commercial alcoholic drinks: beer, white wine and Raki Operational stability: amperometric response for 400 μM ethanol analyzed over 30 days: 1st day 100%, 2nd day response falls up to 85.3% and 10th day response falls up to 21.6% of its initial value. Long-term stability: sensitivity of amperometric calibration towards ethanol analyzed over 8 weeks falls up to 21.2% of its initial value.	[45]
Cu_{52}/Ni_{48}/N-graphene/GCE	Amperometry +0.6 V Electrolyte: 0.10 M NaOH	31.26 μA mM^{-1} cm^{-2} [(31.26 × 10^3 μA M^{-1} cm^{-2})][a]	0.1 mM-N/A [100 μM-N/A][a]	0.2–37.1 mM [(0.2–37.1) × 10^{-3} M][a]	0.9981	Real samples: N/A Operational stability: reproducibility of 10 successive amperometric determination of 5 mM ethanol RSD = 4.2% Long-term stability: amperometric response for 5 mM ethanol analyzed over 1 week stored @ 4 °C: 1st day 100%, 7th day response falls up to 93.7%.	[48]
SPCE-PtNPs	LSV Electrolyte: 1.0 M KOH	0.2757 μA ppm^{-1} (Intercept: 103.95) (12.7 × 10^3 μA M^{-1})	N/A	700–4700 ppm [(0.015–0.102) M][a]	0.999	Real samples: beer and white wine Operational stability: N/A. Disposable electrodes: loss of sensitivity after 3 consecutive measurements: less than 13% Long-term stability: several SPCE-PtNPs prepared and stored @ RT, tested 1st, 7th, 15th and 30th days keeping the response without any appreciable change.	[49]
NiNW array	Amperometry 480 mV Electrolyte: 0.10 M KOH	0.27 μA $μM^{-1}$ cm^{-2} [(0.27 × 10^6) μA M^{-1} cm^{-2}][a]	1.03 μM-N/A	N/A	0.9997	Real samples: N/A Operational stability: N/A Long-term stability: N/A	[38]
GCE-MWCNT-Nf-HRP-SG/Chit-FcAOx-PEI	Amperometry −0.340 mV Electrolyte: 0.10 M KPBS (pH 7.5)	150 ± 0.25 μA mM^{-1} cm^{-2} [(150 ± 0.25) × 10^3 μAM^{-1} cm^{-2}][a]	2.32 ± 0.018 μM-N/A	5–3000 μM [(5–3000) × 10^{-6} M][a]	0.9976	Real samples: beer Operational stability: 90% of the bioelectrode initial activity after 28 successive measurements of 3 mM ethanol during 5 h Long-term stability: ~90% of the bioelectrode original response (measurements @ a regular interval of 3 days) after five weeks stored @ 4 °C and pH 7.5. Biosensor half-life ~184 days.	[46]
CPE 18.0M-NiNWs	Amperometry +0.550 V Electrolyte: 0.10 M NaOH	1372 ± 4 μA M^{-1}	0.31 μM-0.94 μM	(0.1–1.1) × 10^{-4} M	0.9999	Real samples: vodka and cane brandy Operational stability: almost constant up to 5 consecutives test (~1 h) Long-term stability: at least up to 60 days stored at room temperature	This work

Carbon paste electrodes modified with NiO nanodisks (CPE/NiO-NDs). Rosmarinic acid modified screen printed carbon electrode with immobilized alcohol dehydrogenase (ADH) in the presence of NAD^+ cofactor (SPCE/RA/ADH + NAD^+). Cu_{52}/Ni_{48}/N-graphene hybrids modified glass carbon electrode (Cu_{52}/Ni_{48}/N-graphene/GCE). Platinum nanoparticles (PtNPs) modified disposable carbon screen-printed electrode (PtNPs-SPCEs). Nickel nanowires array (NiNW array). Ferrocene entrapped alcohol oxidase (FcAOx) and sol–gel chitosan film coated horseradish peroxidase (HRP) on a multi-walled carbon nanotube (MWCNT) modified glassy carbon electrode (GCE-MWCNT-Nf-HRP-SG/Chit-FcAOx-PEI). Potassium phosphate buffer (KPBS).

[a] Values calculated from the information provided in the references.

was challenged with 20 additions of 20 ppm sulphite solution (Fig. 6 SI B). It is worth mentioning that sulphite anion does not produce any signal even at more elevated concentrations (40 times) than the allowed in food and beverages (up to 10 ppm) [50, 51]. Since distilled alcoholic beverages do not contain neither glucose nor carbohydrates, due to the distillation process that converts them into ethanol and eliminates any trace of them, this sensing system can be applied to the quality control of ethanol level in distilled beverages.

4. Conclusions

We have demonstrated the advantages of a novel nanocomposite (CPE 18.0M-NiNWs) as an electrochemical sensor which allows the highly enhanced non-enzymatic electro-oxidation of ethanol. The proposed nanocomposite sensor evidences outstanding properties that make it an excellent option for efficient ethanol quantification in replacement of enzymatic sensors. CPE 18.0M-NiNWs demonstrates remarkable advantages, among which it is worth mentioning the simple synthesis procedure, low cost, excellent analytical performance in terms of sensitivity, allowing its continuous use during almost 1 h and its storage at room temperature for at least 2 months. These exceptional characteristics make CPE 18.0M-NiNWs an interesting alternative for ethanol content determination in complex samples, such as alcoholic beverages. Beyond the reported results, considering that the highly enhanced non-enzymatic electro-oxidation of ethanol is a hot-topic, and taking into account the outstanding advantages of the composite described here, we believe that this work may be an interesting contribution to future applications in the development of high-performance fuel-cells.

Acknowledgements

The authors are grateful to CONICET (PIP 2015 Project N° 112201501007 10CO), SECyT-UNC (PID Project 2016-2017 SIGEVA N° 30720150101013CB), ANPCyT (Projects: PICT 2013 N° 2817, PICT 2015 N° 0077) and MINCyT-Córdoba (PID Project N° 000018/2014) for the financial support given to this work. C.S.T. and M.L.R. acknowledge doctoral fellowships from CONICET.

Appendix A. Supplementary data

Supplementary data to this article can be found online at https://doi.org/10.1016/j.microc.2018.06.023.

References

[1] F.L. Guest, P.C. Guest, Point-of-care testing and personalized medicine for metabolic disorders, Investig. Early Nutr. Eff. Long-Term Heal. Methods Appl. Methods Mol. Biol. 2018, pp. 105–114, , http://dx.doi.org/10.1007/978-1-4939-7614-0_6.
[2] S. Gupta, C.N. Murthy, C.R. Prabha, Recent advances in carbon nanotube based electrochemical biosensors, Int. J. Biol. Macromol. 108 (2018) 687–703, http://dx.doi.org/10.1016/j.ijbiomac.2017.12.038.
[3] C.M. Pandey, S. Augustine, S. Kumar, S. Kumar, S. Nara, S. Srivastava, B.D. Malhotra, Microfluidics based point-of-care diagnostics, Biotechnol. J. 13 (2018) 1–11, http://dx.doi.org/10.1002/biot.201700047.
[4] P.D. Thungon, A. Kakoti, L. Ngashangva, P. Goswami, Advances in developing rapid, reliable and portable detection systems for alcohol, Biosens. Bioelectron. 97 (2017) 83–99, http://dx.doi.org/10.1016/j.bios.2017.05.041.
[5] V. Bee, C.L. Ee, N. Faizah, M.O.H.D. Aim, E.T. Amiya, M.U.A. Hmed, Trends in paper-based electrochemical biosensors: from design to application, Anal. Sci. 34 (2018), http://dx.doi.org/10.2116/analsci.34.7.
[6] Dhanjai, A. Sinha, L. Wu, X. Lu, J. Chen, R. Jain, Advances in sensing and biosensing of bisphenols: a review, Anal. Chim. Acta 998 (2018) 1–27, http://dx.doi.org/10.1016/j.aca.2017.09.048.
[7] X. Weng, S. Neethirajan, Ensuring food safety: quality monitoring using microfluidics, Trends Food Sci. Technol. 65 (2017) 10–22, http://dx.doi.org/10.1016/j.tifs.2017.04.015.
[8] M. Loh, D. Sarigiannis, A. Gotti, S. Karakitsios, A. Pronk, E. Kuijpers, I. Annesi-Maesano, N. Baiz, J. Madureira, E.O. Fernandes, M. Jerrett, J.W. Cherrie, How sensors might help define the external exposome, Int. J. Environ. Res. Public Health 14 (2017), http://dx.doi.org/10.3390/ijerph14040434.
[9] B.C. Janegitz, T.A. Silva, A. Wong, L. Ribovski, F.C. Vicentini, M.D.P. Taboada Sotomayor, O. Fatibello-Filho, The application of graphene for in vitro and in vivo electrochemical biosensing, Biosens. Bioelectron. 89 (2017) 224–233, http://dx.doi.org/10.1016/j.bios.2016.03.026.
[10] G. Maduraiveeran, W. Jin, Nanomaterials based electrochemical sensor and biosensor platforms for environmental applications, Trends Environ. Anal. Chem. 13 (2017) 10–23, http://dx.doi.org/10.1016/j.teac.2017.02.001.
[11] H.G. Lim, S. Jang, S. Jang, S.W. Seo, G.Y. Jung, Design and optimization of genetically encoded biosensors for high-throughput screening of chemicals, Curr. Opin. Biotechnol. 54 (2018) 18–25, http://dx.doi.org/10.1016/j.copbio.2018.01.011.
[12] W. Qi, X. Zhang, H. Wang, Self-assembled polymer nanocomposites for biomedical application, Curr. Opin. Colloid Interface Sci. 35 (2018) 36–41, http://dx.doi.org/10.1016/j.cocis.2018.01.003.
[13] F. Fathi, R. Rahbarghazi, M.R. Rashidi, Label-free biosensors in the field of stem cell biology, Biosens. Bioelectron. 101 (2018) 188–198, http://dx.doi.org/10.1016/j.bios.2017.10.028.
[14] J. Cui, S. Jia, Organic–inorganic hybrid nanoflowers: a novel host platform for immobilizing biomolecules, Coord. Chem. Rev. 352 (2017) 249–263, http://dx.doi.org/10.1016/j.ccr.2017.09.008.
[15] S. Zhang, R. Geryak, J. Geldmeier, S. Kim, V.V. Tsukruk, Synthesis, assembly, and applications of hybrid nanostructures for biosensing, Chem. Rev. 117 (2017) 12942–13038, http://dx.doi.org/10.1021/acs.chemrev.7b00088.
[16] G. Maduraiveeran, M. Sasidharan, V. Ganesan, Electrochemical sensor and biosensor platforms based on advanced nanomaterials for biological and biomedical applications, Biosens. Bioelectron. 103 (2018) 113–129, http://dx.doi.org/10.1016/j.bios.2017.12.031.
[17] S. Kempahanumakkagari, A. Deep, K.H. Kim, S. Kumar Kailasa, H.O. Yoon, Nanomaterial-based electrochemical sensors for arsenic - a review, Biosens. Bioelectron. 95 (2017) 106–116, http://dx.doi.org/10.1016/j.bios.2017.04.013.
[18] M. Govindhan, B.-R. Adhikari, A. Chen, Nanomaterials-based electrochemical detection of chemical contaminants, RSC Adv. 4 (2014) 63741–63760, http://dx.doi.org/10.1039/C4RA10399H.
[19] B. Hu, Y. Liu, Z.W. Wang, Y. Song, M. Wang, Z. Zhang, C. Sen Liu, Bimetallic-organic framework derived porous Co_3O_4/Fe_3O_4/C-loaded g-C_3N_4 nanocomposites as non-enzymic electrocatalysis oxidization toward ascorbic acid, dopamine acid, and uric acid, Appl. Surf. Sci. 441 (2018) 694–707, http://dx.doi.org/10.1016/j.apsusc.2018.02.093.
[20] S. Deng, P. Yuan, X. Ji, D. Shan, X. Zhang, Carbon nitride nanosheet-supported porphyrin: a new biomimetic catalyst for highly efficient bioanalysis, ACS Appl. Mater. Interfaces 7 (2015) 543–552, http://dx.doi.org/10.1021/am506645h.
[21] K.K. Tadi, R.V. Motghare, V. Ganesh, Electrochemical detection of epinephrine using a biomimic made up of hemin modified molecularly imprinted microspheres, RSC Adv. 5 (2015) 99115–99124, http://dx.doi.org/10.1039/C5RA16636E.
[22] M. Arana, C.S. Tettamanti, P.G. Bercoff, M.C. Rodríguez, Magnetite NPs@C with highly-efficient peroxidase-like catalytic activity as an improved biosensing strategy for selective glucose detection, Electroanalysis 26 (2014) 1721–1728, http://dx.doi.org/10.1002/elan.201400159.
[23] S. Park, S. Park, R.A. Jeong, H. Boo, J. Park, H.C. Kim, T.D. Chung, Nonenzymatic continuous glucose monitoring in human whole blood using electrified nanoporous Pt, Biosens. Bioelectron. 31 (2012) 284–291, http://dx.doi.org/10.1016/j.bios.2011.10.033.
[24] Z. Zhang, P. Pan, X. Liu, Z. Yang, J. Wei, Z. Wei, 3D-copper oxide and copper oxide/few-layer graphene with screen printed nanosheet assembly for ultrasensitive non-enzymatic glucose sensing, Mater. Chem. Phys. 187 (2017) 28–38, http://dx.doi.org/10.1016/j.matchemphys.2016.11.032.
[25] M. Khairy, H.A. Ayoub, C.E. Banks, Non-enzymatic electrochemical platform for parathion pesticide sensing based on nanometer-sized nickel oxide modified screen-printed electrodes, Food Chem. 255 (2018) 104–111, http://dx.doi.org/10.1016/j.foodchem.2018.02.004.
[26] V. Sudha, S.M. Senthil Kumar, R. Thangamuthu, Synthesis and characterization of NiO nanoplatelet and its application in electrochemical sensing of sulphite, J. Alloys Compd. 744 (2018) 621–628, http://dx.doi.org/10.1016/j.jallcom.2018.02.098.
[27] Q. Zhou, A. Umar, E.M. Sodki, A. Amine, L. Xu, Y. Gui, A.A. Ibrahim, R. Kumar, S. Baskoutas, Fabrication and characterization of highly sensitive and selective sensors based on porous NiO nanodisks, Sensors Actuators B Chem. 259 (2018) 604–615, http://dx.doi.org/10.1016/j.snb.2017.12.050.
[28] V.V. Krishnan, Recent developments in metal-supported solid oxide fuel cells, Wiley Interdiscip. Rev. Energy Environ. 6 (2017), http://dx.doi.org/10.1002/wene.246.
[29] X. Xu, X. Liu, B. Xu, A survey of nickel-based catalysts and monolithic reformers of the onboard fuel reforming system for fuel cell APU applications, Int. J. Energy Res. 40 (2016) 1157–1177, http://dx.doi.org/10.1002/er.3509.
[30] Z. Jin, P. Li, Y. Jin, D. Xiao, Superficial-defect engineered nickel/iron oxide nanocrystals enable high-efficient flexible fiber battery, Energy Storage Mater. 13 (2018) 160–167, http://dx.doi.org/10.1016/j.ensm.2018.01.010.
[31] H. Huang, Y. Guo, Y. Cheng, Ultrastable α phase nickel hydroxide as energy storage materials for alkaline secondary batteries, Appl. Surf. Sci. 435 (2018) 635–640, http://dx.doi.org/10.1016/j.apsusc.2017.11.156.
[32] P. Du, Y. Dong, C. Liu, W. Wei, D. Liu, P. Liu, Fabrication of hierarchical porous nickel based metal-organic framework (Ni-MOF) constructed with nanosheets as novel pseudo-capacitive material for asymmetric supercapacitor, J. Colloid Interface Sci. 518 (2018) 57–68, http://dx.doi.org/10.1016/j.jcis.2018.02.010.
[33] X. Yu, M. Wang, A. Gagnoud, Y. Fautrelle, Z. Ren, X. Li, Formation of highly porous $NiCo_2S_4$ discs with enhanced pseudocapacitive properties through sequential ion-exchange, Mater. Des. 145 (2018) 135–143, http://dx.doi.org/10.1016/j.matdes.2018.02.070.

[34] M. Hasan, S.B. Newcomb, J.F. Rohan, K.M. Razeeb, Ni nanowire supported 3D flower-like Pd nanostructures as an efficient electrocatalyst for electrooxidation of ethanol in alkaline media, J. Power Sources 218 (2012) 148–156, http://dx.doi.org/10.1016/j.jpowsour.2012.06.017.

[35] Q. Zhang, C. Zhang, J. Liang, P. Yin, Y. Tian, Orthorhombic α-NiOOH nanosheet arrays: phase conversion and efficient bifunctional electrocatalysts for full water splitting, ACS Sustain. Chem. Eng. 5 (2017) 3808–3818, http://dx.doi.org/10.1021/acssuschemeng.6b02788.

[36] M.S.E. Houache, E. Cossar, S. Ntais, E.A. Baranova, Electrochemical modification of nickel surfaces for efficient glycerol electrooxidation, J. Power Sources 375 (2018) 310–319, http://dx.doi.org/10.1016/j.jpowsour.2017.08.089.

[37] J. Deng, M.R. Nellist, M.B. Stevens, C. Dette, Y. Wang, S.W. Boettcher, Morphology dynamics of single-layered $Ni(OH)_2$/NiOOH nanosheets and subsequent Fe incorporation studied by in situ electrochemical atomic force microscopy, Nano Lett. 17 (2017) 6922–6926, http://dx.doi.org/10.1021/acs.nanolett.7b03313.

[38] S. Blanco, R. Vargas, J. Mostany, C. Borrás, B.R. Scharifker, A novel nickel nanowire amperometric sensor: direct current vs. alternating current strategies for ethanol, acetaldehyde and acetylcholine detection, J. Electroanal. Chem. 740 (2015) 61–67, http://dx.doi.org/10.1016/j.jelechem.2014.12.028.

[39] L. Xu, Z. Wang, X. Chen, Z. Qu, F. Li, W. Yang, Ultrathin layered double hydroxide nanosheets with Ni(III) active species obtained by exfoliation for highly efficient ethanol electrooxidation, Electrochim. Acta 260 (2018) 898–904, http://dx.doi.org/10.1016/j.electacta.2017.12.065.

[40] M.M.P.S. Neves, M.B. González-García, D. Hernández-Santos, P. Fanjul-Bolado, Streptavidin functionalized nickel nanowires: a new ferromagnetic platform for biotinylated-based assays, Talanta 144 (2015) 283–288, http://dx.doi.org/10.1016/j.talanta.2015.05.085.

[41] C. Schönenberger, B.M.I. van der Zande, L.G.J. Fokkink, M. Henny, C. Schmid, M. Krüger, A. Bachtold, R. Huber, H. Birk, U. Staufer, Template synthesis of nanowires in porous polycarbonate membranes: electrochemistry and morphology, J. Phys. Chem. B 101 (1997) 5497–5505, http://dx.doi.org/10.1021/jp963938g.

[42] R.S. Schrebler Guzmán, J.R. Vilche, A.J. Arvía, The kinetics and mechanism of the nickel electrode-III. The potentiodynamic response of nickel electrodes in alkaline solutions in the potential region of $Ni(OH)_2$ formation, Corros. Sci. 18 (1978) 765–778, http://dx.doi.org/10.1016/S0010-938X(78)80094-8.

[43] X.K. Tian, X.Y. Zhao, L. De Zhang, C. Yang, Z.B. Pi, S.X. Zhang, Performance of ethanol electro-oxidation on Ni-Cu alloy nanowires through composition modulation, Nanotechnology 19 (2008), http://dx.doi.org/10.1088/0957-4484/19/21/215711.

[44] Y. Yu, M. Guo, M. Yuan, W. Liu, J. Hu, Nickel nanoparticle-modified electrode for ultra-sensitive electrochemical detection of insulin, Biosens. Bioelectron. 77 (2016) 215–219, http://dx.doi.org/10.1016/j.bios.2015.09.036.

[45] M. Bilgi, E. Merve, E. Ayranci, Sensor and biosensor application of a new redox mediator: rosmarinic acid modified screen-printed carbon electrode for electrochemical determination of NADH and ethanol, J. Electroanal. Chem. 813 (2018) 67–74, http://dx.doi.org/10.1016/j.jelechem.2018.02.012.

[46] S.R. Chinnadayyala, A. Kakoti, M. Santhosh, P. Goswami, A novel amperometric alcohol biosensor developed in a 3rd generation bioelectrode platform using peroxidase coupled ferrocene activated alcohol oxidase as biorecognition system, Biosens. Bioelectron. 55 (2014) 120–126, http://dx.doi.org/10.1016/j.bios.2013.12.005.

[47] K.-L. Wu, B.-B. Jiang, Y.-M. Cai, X.-W. Wei, X.-Z. Li, W.-C. Cheong, Efficient Electrocatalyst for Glucose and Ethanol Based on Cu/Ni/N-Doped Graphene Hybrids, ChemElectroChem 4 (6) (June 2017) 1419–1428, http://dx.doi.org/10.1002/celc.201700078 (First published: 08 March 2017).

[48] M.M. Pereira Silva Neves, M.B. González-García, P. Bobes-Limenes, A. Pérez-Junquera, D. Hernández-Santos, F.J. Vidal-Iglesias, J. Solla-Gullón, P. Fanjul-Bolado, A non-enzymatic ethanol sensor based on a nanostructured catalytic disposable electrode, Anal. Methods 9 (2017) 5108–5114, http://dx.doi.org/10.1039/C7AY01078H.

[49] H. Nakamura, R. Tanaka, K. Suzuki, M. Yataka, Y. Mogi, A direct determination method for ethanol concentrations in alcoholic beverages employing a eukaryote double-mediator system, Food Chem. 117 (2009) 509–513, http://dx.doi.org/10.1016/j.foodchem.2009.04.026.

[50] S. Preecharueangrit, P. Thavarungkul, P. Kanatharana, A. Numnuam, Amperometric sensing of sulfite using a gold electrode coated with ordered mesoporous carbon modified with nickel hexacyanoferrate, J. Electroanal. Chem. 808 (2018) 150–159, http://dx.doi.org/10.1016/j.jelechem.2017.11.070.

[51] C. Ruiz-Capillas, F. Jiménez-Colmenero, Application of flow injection analysis for determining sulphites in food and beverages: a review, Food Chem. 112 (2009) 487–493, http://dx.doi.org/10.1016/j.foodchem.2008.05.085.

[52] A. Isaac, J. Davis, C. Livingstone, A.J. Wain, R.G. Compton, Electroanalytical methods for the determination of sulfite in food and beverages, TrAC Trends Anal. Chem. 25 (2006) 589–598, http://dx.doi.org/10.1016/j.trac.2006.04.001.